Direct observation and structural characterization of natural and metal ion-exchanged HEU-type zeolites

Reference:

Filippousi Maria, Turner Stuart, Katsikini Maria, Pinakidou Fani, Zamboulis Demetris, Pavlidou Eleni, van Tendeloo Gustaaf.- Direct observation and structural characterization of natural and metal ion-exchanged HEU-type zeolites
Microporous and mesoporous materials: zeolites, clays, carbons and related materials - ISSN 1387-1811 - 210(2015), p. 185-193
DOI: http://dx.doi.org/doi:10.1016/j.micromeso.2015.01.043
Handle: http://hdl.handle.net/10067/1260060151162165141

Direct observation and structural characterization of natural and metal ion-exchanged HEU-type zeolites.

Maria Filippousi[1]*, Stuart Turner[1],
Maria Katsikini[2], Fani Pinakidou[2], Demetris Zamboulis[3], Eleni Pavlidou[2],
Gustaaf Van Tendeloo[1]

Corresponding Author*

1 *EMAT, University of Antwerp, Groenenborgerlaan 171, B-2020 Antwerp, Belgium.*

2 *Solid State Physics Section, Physics Department, Aristotle University of Thessaloniki, GR-54124, Thessaloniki, Greece.*

3 *Laboratory of General and Inorganic Chemical Technology, Department of Chemistry, Aristotle University of Thessaloniki, GR-54124 Thessaloniki, Greece.*

Abstract

The atomic structure of natural HEU-type zeolite and two ion-exchanged variants of the zeolite, Ag^+ (Ag-HEU) and Zn^{2+} (Zn-HEU) ion exchanged HEU-type zeolites, are investigated using advanced transmission electron microscopy techniques in combination with X-ray powder diffraction and X-ray absorption fine structure measurements. In both ion-exchanged materials, the loading of the natural HEU zeolite is confirmed.

Using low-voltage, aberration-corrected transmission electron microscopy at low-dose conditions, the local crystal structure of natural HEU-type zeolite is determined and the interaction of the ion-exchanged natural zeolites with the Ag^+ and Zn^{2+} ions is studied. In the case of Ag-HEU, the presence of Ag^+ ions and clusters at extra-framework sites as well as Ag nanoparticles has been confirmed. The Ag nanoparticles are preferentially positioned at the zeolite surface. For Zn-HEU, no large Zn(O) nanoparticles are present, instead, the HEU channels are evidenced to be decorated by small Zn(O) clusters.

Key Words: HEU-type zeolite; ion-exchange; aberration corrected transmission electron microscopy; XRPD; EXAFS.

* Corresponding author. Tel.:+32 3 265 35 29, fax: +32 3 265 33 18

E-mail address: Maria.filippousi@uantwerpen.be

1. Introduction

HEU-like zeolites are three-dimensional framework structures consisting of $(Si,Al)O_4$ tetrahedra, in which each oxygen is shared between two neighboring tetrahedra. Substitution of Si^{4+} by Al^{3+} results in a deficiency of positive charge in the zeolite framework. The net negative charge produced is usually balanced by cations, mainly Na^+, K^+, and Ca^{2+} for natural zeolites, which are situated in the cavities within the structure. [1-3] These extra-framework cations are mobile and can therefore be exchanged by other metal ions. Zeolites are known to have high cation exchange and adsorption capacities; generally, zeolite cation exchange capacities (CEC) are a factor of two to three higher than those of most smectites and vermiculites. [4] Furthermore, as zeolite pores are a natural consequence of the zeolite crystal structure, they possess a constant geometry. This constant geometry combined with their high specific surface area is of interest for applications such as catalysis and molecular sieving (straight and branched hydrocarbons). The cavities and channels in zeolites can also serve as hosts for e.g. metals or metal-oxide clusters or nanoparticles, forming novel composite materials. [5] The wider the zeolite channels, the larger the clusters that can be introduced into the structure.

Natural zeolites have attracted worldwide interest for use in a broad range of applications, even though they may contain more impurities as compared to their synthetic counterparts. Many of these applications are in medicine, as natural zeolites are generally cheaper and less toxic than their synthetic counterparts. Since natural zeolites are abundant in nature, they are easily available and environmental friendly. [6-9] HEU-type zeolites (clinoptilolite and heulandite; monoclinic crystal structure, space group C2/m, cell parameters a≈17.7, b≈17.9 and c≈7.4 Å [10]) are the most abundant minerals on earth exhibiting a zeolite structure, making them low-cost

industrial minerals with several commercial applications. [1,11] According to the Zeolite Subcommittee of the Commission on New Minerals and Mineral Names of the International Mineralogical Association, heulandite is defined as the zeolite mineral which has the framework topology of heulandite and a ratio Si/Al < 4, while clinoptilolite is defined as the series with the same framework topology but with Si/Al > 4. [1] For clarity, in this manuscript our natural zeolite will be referred to as HEU-type zeolite, even though the Si/Al ratio in our samples is always in correspondence with heulandite. (See supplementary information).

Transmission electron microscopy (TEM) is a valuable technique for the characterization of zeolites, [12] as important information such as crystal/defect structure [13,14] and identification of loaded materials like metal or metal-oxide nanoparticles inside the matrix, [15,16] can be derived from TEM data. The problem with TEM characterization of natural zeolites is that they generally contain a large amount of water. Degradation of the zeolite structure under electron beam irradiation, caused mainly by radiolysis, occurs very fast and makes it extremely difficult to acquire HRTEM images and consequently perform a full structural characterization based upon these data. Being able to perform stable TEM measurements would be of especially great value in the characterization of modified HEU-type zeolites, ion-exchanged with extra-framework guests like metallic cations or clusters through the use of e.g. ion exchange. In this type of loaded zeolite materials, knowledge on the size, shape and distribution of the constituting ions/clusters/nanoparticles would then be directly accessible by TEM.

In this work, we report the first characterization of the atomic structure of a HEU-type zeolite through use of low voltage aberration corrected transmission electron microscopy under low dose conditions. [17, 18] The sensitivity of this type of zeolite

to the electron beam is in the typical range for natural zeolites and therefore the described measuring procedures for TEM imaging of intact HEU-type zeolites are applicable to many other sensitive, natural zeolites. This will provide a deeper understanding of the structure of the zeolite and the interaction of exchanged ion or clusters with the framework pores. As Diaz &Mayoral [20] reported, there are only few studies which have focused on the observation of guest materials within a zeolite structure through use of low electron dose conditions and short exposure times. [19, 20] We will also provide more information on the morphological and structural properties of the HEU-type zeolite after ion exchange with Ag^{+} and Zn^{2+} ions by combining the TEM data with X-ray powder diffraction (XRPD) and X-ray absorption fine structure (XAFS) spectroscopy. The element selective character of the latter allows the determination of the bonding environment of the exchanged ions (in this case for Zn^{2+}), irrespective of the crystalline or amorphous character of the host lattice, and has previously already been used for the study of Zn-exchanged zeolites. [21,22]

2. Experimental

Pure faintly-white natural HEU-type zeolite crystals and crystals ion-exchanged with Ag^{+} and Zn^{2+} were used in this work. The Zn- and Ag-exchanged forms of the HEU-type zeolite crystals (indicated/denoted as Zn-HEU and Ag-HEU respectively) were prepared in two steps; (1) the preparation of a Na homoionic form of the zeolite and (2) Na-exchange with Zn- and Ag-ions.

In order to prepare the Na homoionic form used as precursor for Zn-HEU, 1g of the pulverized raw materials was treated for 24 hours with 50 mL of 2M NaCl solution

under refluxing. For the Na homoionic form used as precursor for Ag-HEU, only 0.65g of pulverized raw material was treated with the same procedure.

The Na homoionic forms of the zeolite were separated by centrifugation, washed with double distilled water until they become Cl^- free and finally dried at 70°C. A quantity of about 0.50 g of the prepared Na homoionic forms of the HEU-type zeolite crystals was treated under refluxing for 24 h with 50 mL of a 0.5 M $Zn(NO_3)_2*4H_2O$ and for 24 h with 50 mL of a 0.3 M $AgNO_3$ solution for the preparation of its Zn-HEU and Ag-HEU forms respectively. After separation of the solid from the liquid phase by centrifugation, the Zn-HEU and Ag-HEU were washed with double distilled water and dried at 80°C. The reagents used for the preparation of the Na- form of the HEU-type zeolite, Zn-HEU and Ag-HEU forms (NaCl, $Zn(NO_3)_2*4H_2O$ and $AgNO_3$) were of analytical grade and used without further purification.

Samples suitable for TEM and high-angle annular dark-field scanning transmission electron microscopy (HAADF-STEM) were prepared by mechanical grinding and polishing the HEU-type zeolite crystals followed by ion milling in a Balzers Ar^+ ion mill. High resolution TEM (HRTEM) and HAADF-STEM images were acquired on an aberration-corrected FEI Titan 'Cubed' microscope operated at 80kV. In order to minimize beam damage to the sample, all images were acquired using a low electron dose in the range of 50-150 $e/Å^2 s$. The exposure time in TEM was limited to 0.1 s, and a beam blanking system was used in between acquisitions to minimize exposure of the sample to the electron beam. Image simulations were performed using the JEMS software package. Fourier filtering in Figure 4 was performed using the Digital Micrograph software suite. Tomography series were acquired on a FEI Tecnai G2 microscope, operated at 200 kV acceleration voltage in STEM mode with an angular range from -70º to +65º for Zn-HEU and -70º to +70º

for the Ag-HEU with a tilt increment of 5º, in order to minimize beam damage. A Fischione tomography holder (model 2020) was used and the series were acquired automatically using the Xplore3D software. The alignment of the series was performed with the Inspect 3D software. 3D reconstruction was performed using the Simultaneous Iterative Reconstruction Technique (SIRT) as implemented in the Inspect 3D software package (FEI Company).

XRPD analysis of the materials was performed using a Philips PW1710 diffractometer with Ni-filtered Cu-Ka radiation operating at 40kV and 30mA. The unit cell parameters of the HEU-type zeolite were refined by the Le Bail fitting of the XRPD data using the JANA2006 software [23].

The X-ray Absorption Fine Structure (XAFS) spectra were recorded at the Zn-K-edge at the KMC-II beamline of the BESSY-II storage ring of the Helmholtz Zentrum Berlin. The beamline is equipped with a double SiGe (111) graded-crystal monochromator and a Röntec XFlash fluorescence detector that was used in order to electronically discriminate the Zn K_α photons. The detector was positioned in the horizontal plane at right angle to the incident beam. The angle of incidence was 80^o to the sample surface. A ZnO powder sample was used as reference material after proper corrections for self-absorption. The spectra were normalized with the signal of an ionization chamber positioned in front of the sample. A Zn thin foil measured in the transmission mode was used for the correction of the energy shifts induced by the monochromator and as a reference material.

3. Results and discussion.

3.1. Structural characterization of the pure HEU-type zeolite

To date, the main technique to study the structure of natural HEU-type zeolites has been single crystal X-ray diffraction. [1] However, XRPD collects structural

information from a large area to reveal an average structure, and therefore does not provide local information. In order to gain more information on the pure HEU-type zeolite at a local level, low voltage aberration corrected TEM was used in this study. To keep the HEU framework from collapsing under the electron beam illumination, high resolution images were acquired from different crystal projections, while keeping the electron dose as low as possible through use of a low intensity beam and the lowest possible magnification. A beam blanking system was also used in between acquisitions to minimize exposure of the sample to the electron beam.

In Figure 1, high resolution TEM images of the HEU-type zeolite are presented along five different zone axes, which allowed us to confirm, based on the XRPD measurements, the monoclinic structure of the HEU-type zeolite. Both Cowley&Moodie and Kremer *et al.* [24, 25] reported that upon use of heavy under-focus conditions, tunnels or pores (less dense structures) will appear as bright contrast, while dense material within the sample will give rise to dark contrast. In our case the HRTEM images were taken at relatively large under-focus conditions, meaning white contrast features in the images should be the zeolite pores. To confirm this interpretation, we performed detailed image simulation for the [010] orientation of the sample at appropriate defocus and thickness values. The image simulation is displayed on Figure 2 and is based on the structure model with C2/m space group, as deduced from X-ray diffraction measurements in the literature. [10] The simulation confirms our interpretation that the bright contrast features in the HRTEM images correspond to the least dense areas in the framework (double oxygen columns).

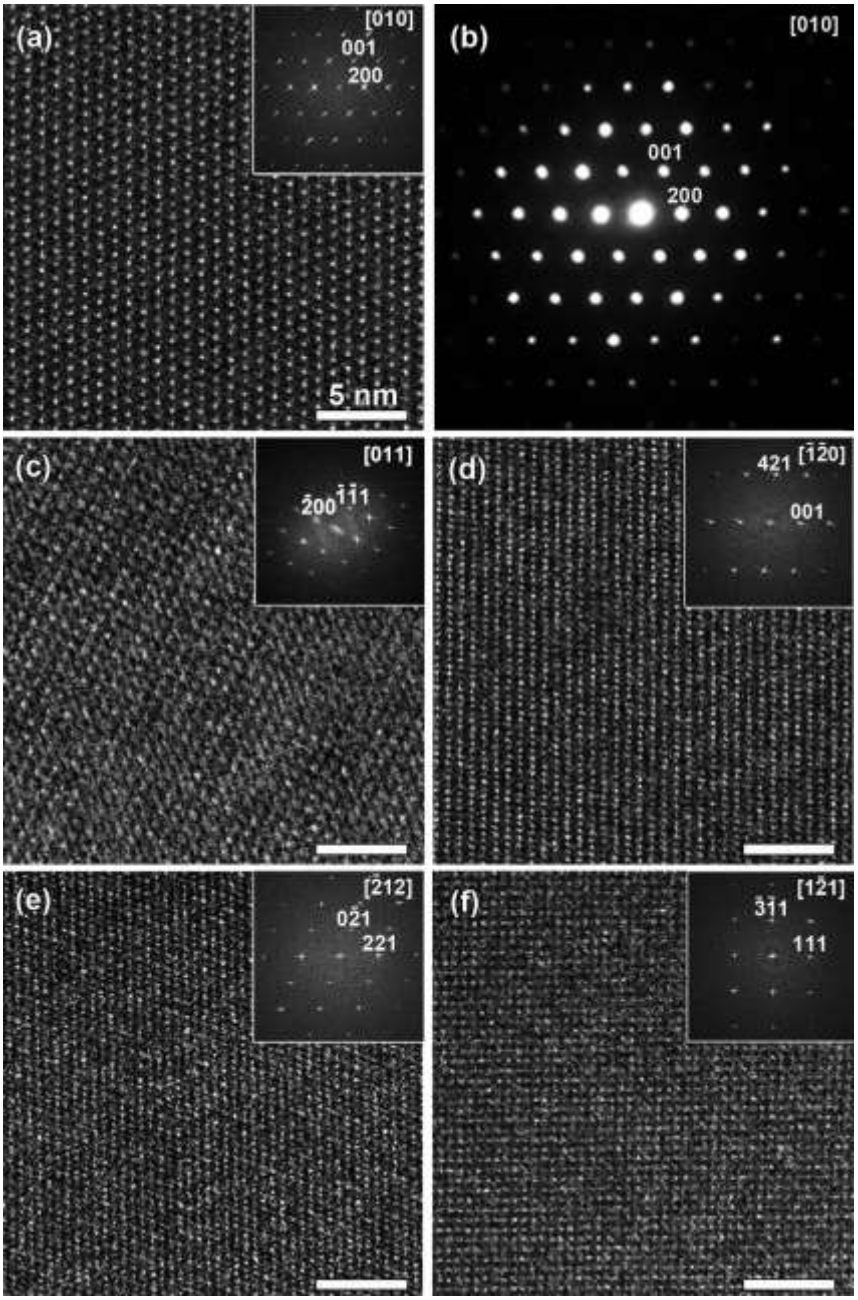

Figure 1: *HRTEM images of the HEU-type zeolite, along a) [010], c) [011], d) [-1-20], e) [-212] and f) [1-21] zone axes together with their FT patterns shown as an inset on the top right. b) A SAED pattern from the region shown in figure a. The scale is identical in all high resolution images.*

In Figure 2a, an HRTEM image along the [010] zone axis together with the corresponding image simulation for a defocus value of 150 nm under focus and a thickness of 67 nm are presented. In Figure 2b, a structural model of the HEU-type zeolite oriented along the [010] zone axis is overlaid to the magnified image simulation. The simulation is in good agreement with the experiment, even though the image acquisition was carried out under minimal electron dose and using a short exposure time of 0.1 s.

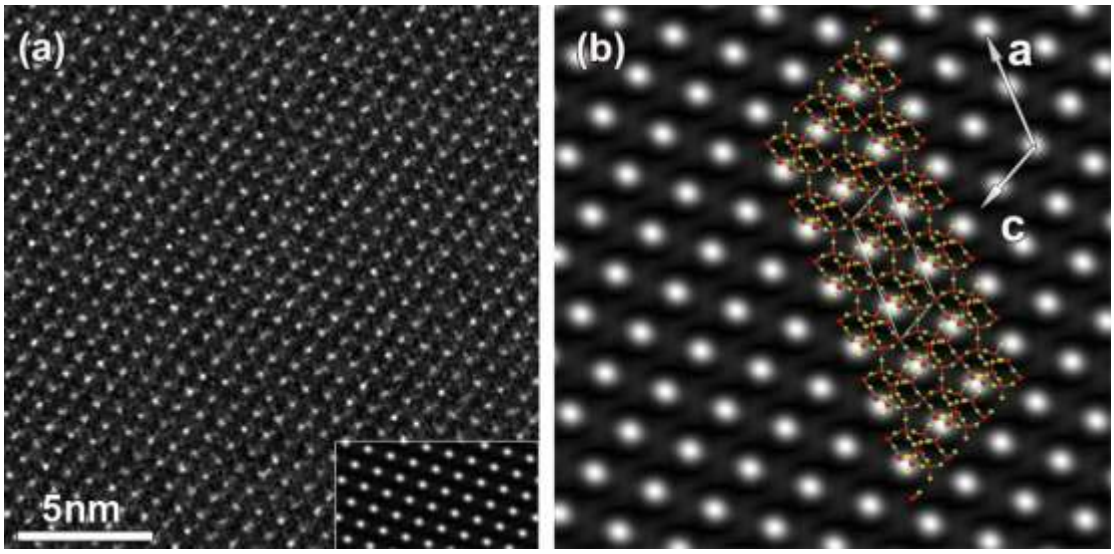

Figure 2: *(a) HRTEM image of the HEU-type zeolite along [010]. A simulated image at Δf = -150 nm and thickness 67 nm is presented as an inset. (b) A model of the HEU-type zeolite along [010] overlaid on the magnified image simulation.*

3.2 Characterization of the HEU-type zeolite after ion exchange with Ag^{+} and Zn^{2+} -ions:

XRPD patterns were taken for the HEU-type zeolite before and after ion-exchange with metals (Figures SI 2,3). The refined unit cell parameters of the HEU-type zeolite are as follows: *C*2/*m* space group, *a* = 17.754(1) Å, *b* = 17.934(1) Å, *c* = 7.4364(5) Å, β = 116.38(1)º. These values are close to the parameters of other zeolites with the

HEU-type structure (for example, PDF#77-0339). On the XRPD pattern of the Ag-HEU sample we can notice that the most intensive 020 peak ($2\theta \approx 10^{o}$) is split into two sub-peaks. Since there are no admixtures that can be attributed to this peak, we believe that one of the peaks corresponds to the (020) reflection of the Ag-exchanged HEU-type zeolite and the other to the (020) reflection of the raw HEU. However, the laboratory XRPD data is insufficient for an accurate determination of the cell parameters of these two phases due to the strong overlap of the peaks. In case of the Zn-HEU, there is one reflection around 10º, but it is significantly broadened in comparison to the HEU-type zeolite. Therefore, it is reasonable to conclude that this sample also consists of two phases: a Zn^{2+} exchanged HEU-type zeolite and the raw HEU-type zeolite, but their unit cell parameters are very close which results in a single broadened peak. This means that both the Ag-HEU and Zn-HEU samples contain an ion-exchanged and a raw HEU-type zeolite phase. Typically the treatment of HEU with Ag^{+} and Zn^{2+} ions does not affect the zeolite crystal structure [3, 26], and we expect similar results in this work.

Since there are no extra reflections in the XRPD patterns which can be attributed to the presence of significant amounts of Ag/AgO_x or Zn/ZnO phases, the Ag^{+} and Zn^{2+} ions are expected to be exchanged into the HEU-type zeolite structure, which is characterized by the presence of five distinct extra-framework sites (A1, A2, A3, B and C) (see supplementary information) that may host a variety of exchangeable cations. [3]

However, the presence or absence of small nanoparticles or clusters after ion exchange cannot be ruled out by XRPD alone. Small amounts of crystalline Ag/AgO_x or Zn/ZnO nanoparticles in the ion-exchanged material will not generate easily visible

reflexes in the XRPD pattern, due to peak broadening as a consequence of their small size. Therefore, to confirm or rule out the presence of small clusters or nanoparticles in the ion-exchanged materials, electron microscopy imaging was carried out.

Figure 3a and 3b are two HAADF-STEM (Z-contrast) images of sample Ag-HEU and Zn-HEU respectively. EDX spectra taken from the materials clearly show the presence of Ag for Ag-HEU and Zn for Zn-HEU, indicating the materials were partially ion-exchanged (Figure 4c and d, EDX elemental analysis are presented in the supplementary information). From the Z-contrast image of Ag-HEU it is immediately obvious that larger Ag-containing nanoparticles have (also) been formed during the ion-exchange procedure. High resolution TEM imaging evidences that these larger nanoparticles are crystalline Ag (see supplementary information). The presence or absence of small Ag clusters can however not be made out from these images. In the case of Zn-HEU, the contrast in the HAADF-STEM image is totally different. The image contrast is uniform, excluding the presence of larger nanoparticles as in Ag-HEU. However, as discussed above, the EDX spectrum of Zn-HEU clearly indicates that Zn is present in the Zn-HEU material.

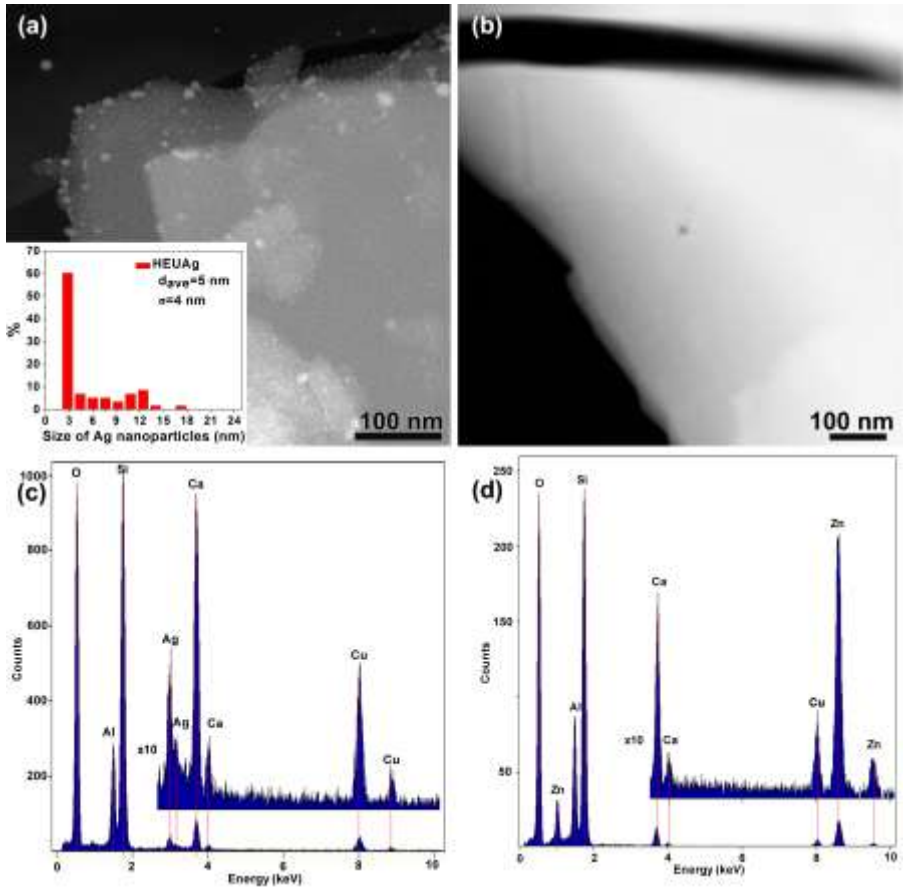

Figure 3: *(a) HAADF-STEM image of Ag-HEU together with a size distribution of the Ag nanoparticles visible in the image. (b) HAADF-STEM image of the Zn-HEU, (c) and (d) EDX spectra of the Ag-HEU and Zn-HEU respectively. The Cu signal arises from the Cu grid used*

In order to study the possible presence of small clusters in the channels of the ion-exchanged Ag-HEU and Zn-HEU material, we used HRTEM imaging under low-dose conditions. A typical image of the Ag-HEU sample, oriented along the [010] zone axis orientation, is displayed in Figure 4a. Preferential growth of (010) planes in the the natural zeolite sample mean this zone axis is the most frequently observed in the as-prepared sample. Careful observation of the image, and comparison to the data acquired from the empty HEU-type zeolite appears to reveals the presence of very small Ag clusters through extra dark-contrast spots that were not present in the case of the empty framework. To accurately determine the size of the Ag clusters, we

removed the influence of the HEU lattice by applying a Fourier filtering technique to the HRTEM image, resulting in the image in Figure 4b. This type of Fourier filtering has previously been successfully used for the imaging of nanoparticles on graphene supports. [27] By "removing" the HEU lattice, the size and shape of the Ag clusters becomes apparent. All Ag clusters are smaller than 1 nm in diameter and are therefore similar in size to the HEU pores (largest pore diameter = 0.6 nm). The fact that the clusters have a similar size to the HEU pores, makes it highly likely that they are indeed embedded inside the HEU zeolite host. Figure 4b reveals that the Ag clusters are initially well-distributed throughout the micropores of the zeolite host. Immediately after the first HRTEM image in Figure 4a, a second HRTEM image of the same region was acquired, which is displayed in Figure 4c. Note that in between image acquisitions, the electron beam was blanked to spare the sample. It is clear that the short exposure of the HEU lattice to the electron beam has started to damage the HEU lattice. We applied the same Fourier filtering technique to this image, resulting in Figure 4d. The Ag nanoparticles in this image are visibly larger than those in Figure 4b. The exposure of the material to the electron beam has in other words resulted in a local destruction of the HEU lattice, and an agglomeration of the embedded Ag nanoparticles. A third and final image of the Ag-HEU is displayed in Figure 4e. After just three short exposures, the HEU lattice is completely destroyed, and the Ag nanoparticles have agglomerated into larger 2-5 nm structures under electron beam irradiation. These structures are even better visible in the low-pass filtered image, displayed in Figure 4f.

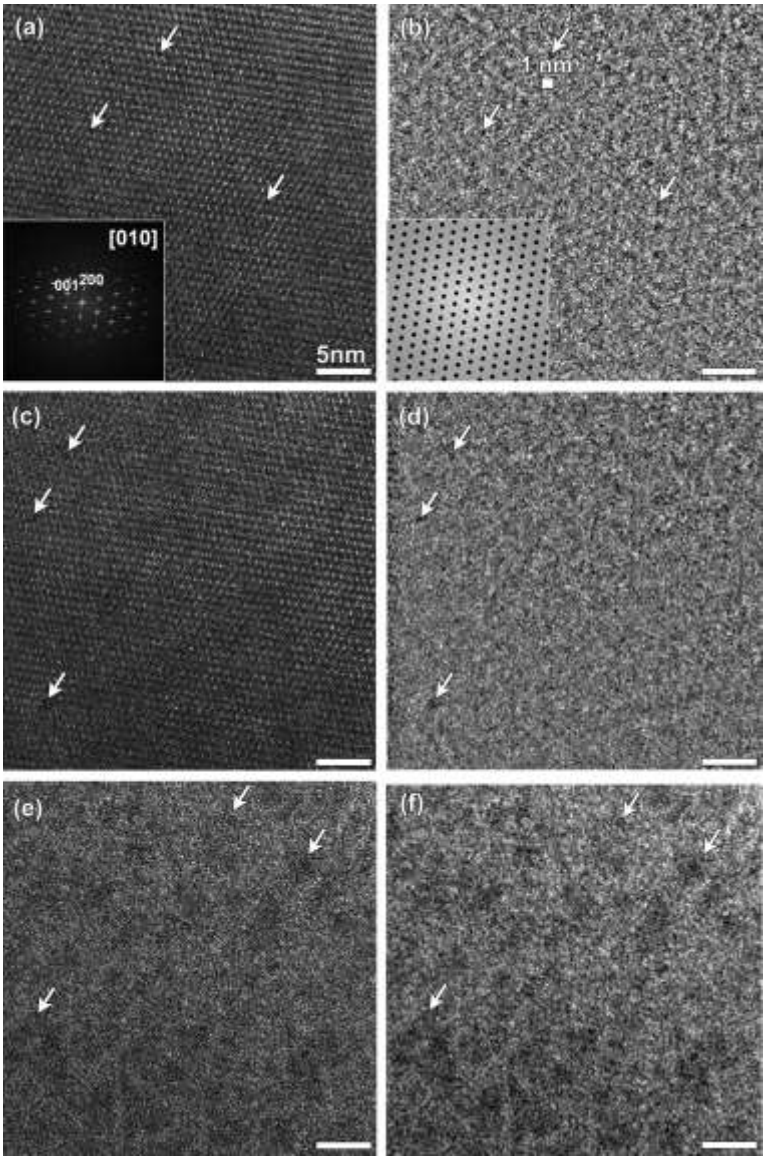

Figure 4:*(a) HRTEM image of Ag-HEU . The inset FT evidences the [010] orientation of the sample. (b) Low-pass filtered HRTEM image from (a) with the HEU lattice removed by Fourier-filtering. The mask used to subtract the HEU lattice is shown as inset. Several small Ag clusters are visible (black dots, indicated by arrows).The indicated scale bar is 1nm (c) Second exposure of the same Ag-HEU (d) Low-pass filtered HRTEM image from (c) with the HEU lattice removed by Fourier-filtering. The Ag clusters have visibly grown in size. (e) Third exposure of the same sample, the HEU lattice is completely destroyed. (f) Low-pass filtered HRTEM image of (e), showing the presence of agglomerated Ag clusters. The scale is identical in all images. Fourier filtering for Figure 5b and 5d was performed by masking the Fourier components corresponding to the HEU lattice in the FT's of images 5a and 5c respectively, and inverse Fourier transforming the masked images. Figures 5b, 5d and 5f were low-pass filtered for clarity.*

The same procedure was followed for the Zn-HEU sample, in order to confirm or rule out the presence of small Zn(O) clusters inside the zeolite. As can be seen from Figure 5a, dark-contrast features, similar to those observed in the Ag-HEU sample, are observed in the high resolution images. In analogy to the Ag clusters, these dark contrast features are small Zn(O) clusters, that are likely positioned inside the HEU pores. Similar to the Ag clusters in Ag-HEU, the Zn(O) clusters grow under the electron beam irradiation, and are more visible after the first exposure due to the amorphization of the HEU lattice. The nature of these small Zn(O) clusters will be discussed in detail in the XAFS section below. [28]

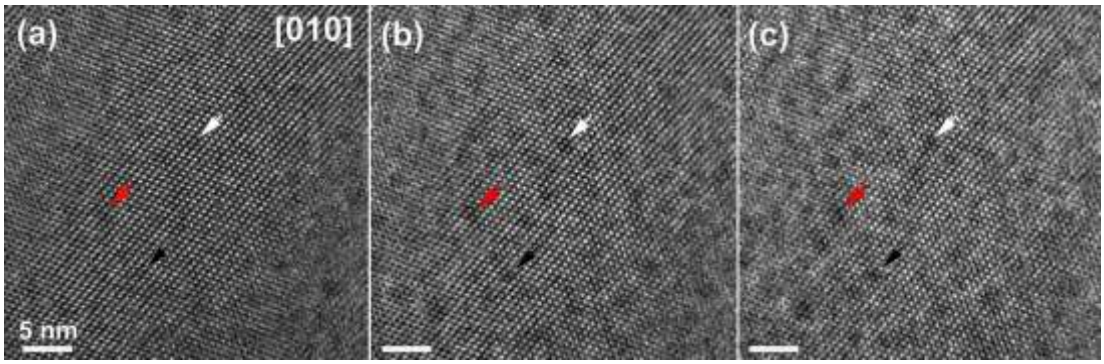

Figure 5: *(a) HRTEM image of Zn-HEU. Several small Zn(O) clusters are visible (black dots, indicated by arrows). (b) Second exposure of the same Zn-HEU. The Zn(O) clusters are more clearly visible due to the amorphisation of the HEU lattice. (c) Third consecutive exposure of the Zn-HEU sample. The Zn(O) clusters appear to have grown. The scale is identical in all images.*

Although TEM is a powerful technique for the study of nanomaterials, it can only provide 2D projections of 3D objects. In order to reveal the exact positioning of the Ag and Zn(O) material in the zeolite volume, electron tomography can be used. In this technique, the sample is tilted over a wide tilt range inside the electron microscope

and images are acquired at few degree intervals. These acquired images are used as an input for a tomographic reconstruction, yielding a 3D representation of the object. [29, 30] We performed electron tomography measurements on both the Zn-HEU and the Ag-HEU samples, with the microscope operated in Z-contrast STEM mode. In the case of Ag-HEU, the largest Ag nanoparticles, seen in HAADF-STEM images of the sample in Figure 6a, are located at the surface of the zeolite. Smaller clusters are present inside the zeolite host. Similar tomography measurements were also carried out for the Zn-HEU. The results reveal that the Zn(O) clusters appear brighter when compared to the zeolitic matrix (Figure 6b). The slice through the tomographic reconstruction in Figure 6f shows that the Zn(O) clusters are inside the volume of the HEU-type zeolite.

Although a certain degree of framework collapse has certainly taken place under the extended electron beam illumination needed for electron tomography, the clusters and nanoparticles seen in the reconstruction should not have moved far from their initial position. This means we can conclude that small Ag clusters are initially inside the zeolite host and not at the surface. Only the largest Ag nanoparticles seen in the HAADF-STEM images are present at the Ag-HEU surface.

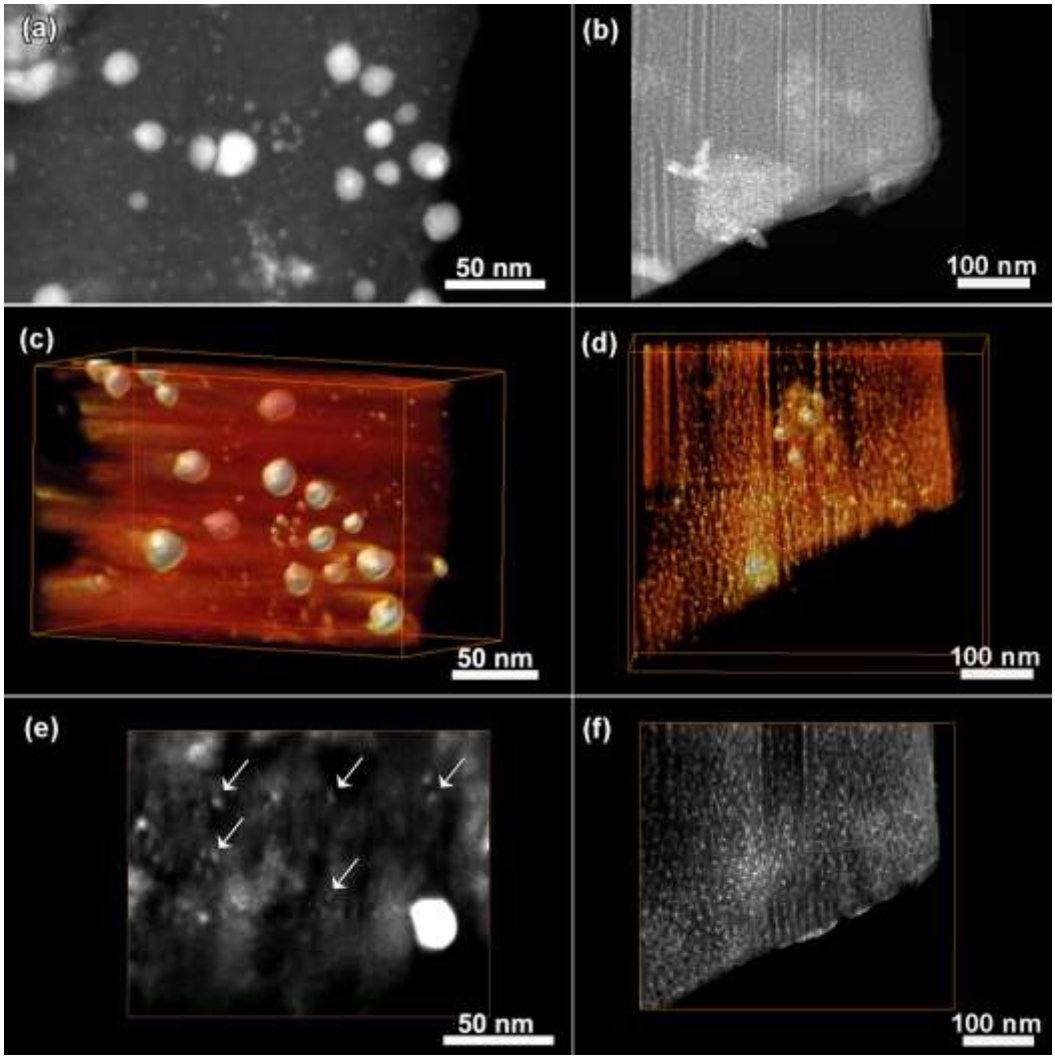

Figure 6: *HAADF-STEM images of (a) Ag-HEU and (b) Zn-HEU. (c) 3D representation of the reconstructed volume of the Ag-HEU (d) 3D representation of the reconstructed volume of the Zn-HEU (e) Orthoslices through the reconstructed volume of the Ag-HEU sample. The largest Ag nanoparticles are formed at the surface of the zeolite during synthesis. The smaller nanoparticles, indicated by arrows around 1-6 nm in diameter, are present inside the zeolite host (f) Orthoslices through the reconstructed volume of the Zn-HEU sample. The bright regions correspond to Zn(O)clusters positions, which are located in the middle of the volume.*

To further investigate the nature of the Zn(O) clusters in the Zn-HEU material, the bonding environment of Zn^{2+} was studied by means of XAFS spectra recorded at the

Zn-K-edge. The $\chi(k)$ spectra, of the Zn-HEU , the ZnO powder and metallic Zn obtained after atomic background subtraction of the EXAFS spectra and transformation from the energy space to the k-space, are shown in Figure 7a along with the corresponding Fourier Transforms (FT) shown in Figure 7b. The fitting was performed using the FEFFIT program [31] and the photoelectron scattering paths were calculated using the FEFF8 code. [32] The spectra of the Zn-HEU and ZnO reference were fitted using the model of ZnO (S.G.: P 6_3 m c, a= 3.25 Å, c=5.21 Å) whereas in the case of the Zn foil the Zn metal structure (S.G.: P 6_3/m m c, a= 2.66 Å, c=4.95 Å) was used as a model. The coordination numbers of Zn in the ZnO and Zn foil reference samples were kept fixed to the values predicted by the model, whereas the nearest neighbor (nn) distances and the Debye-Waller factors were allowed to vary. The energy origin and the amplitude reduction factor were commonly iterated for all the nn shells of each sample. Importantly, in the case of Zn-HEU, the absence of peaks in the FT beyond the 1^{st} nn shell indicates that Zn neither occupies positions in the host zeolite lattice nor forms separate ZnO phases. Therefore, the fitting was performed using only one nn scattering path and more specifically the first path from the ZnO model. During the fitting of the Zn-HEU EXAFS spectrum, the energy origin and the amplitude reduction factor were kept fixed to the values determined form the ZnO reference sample while the nn distance, coordination number and Debye-Waller factor were iterated. The fitting results are listed in Table I.

Table I: *Fitting results of the EXAFS analysis. N, R, σ^2, ΔE and S_0^2 correspond to the coordination number, the nearest neighbor distance, the Debye-Waller factor, the energy origin and the amplitude reduction factor, respectively. The errors reported are the uncertainties provided by the FEFFIT program.*

Sample	**Atom pair**	**N**	**R (Å)**	**$\sigma^2 \times 10^{-3}$ (Å^2)**	**ΔE (eV)**	S_0^2
Zn-HEU	Zn-O	6.2 ± 0.5	2.07 ± 0.01	10.1 ± 1.7	-1.3	0.79
ZnO	Zn-O	4	1.96 ± 0.01	4.9 ± 0.8		
	Zn-Zn	12	3.22 ± 0.01	8.9 ± 0.5		
	Zn-O	9	3.76 ± 0.02	7.0 ± 1.8	-1.3 ± 0.5	0.79 ± 0.04
	Zn-Zn	6	4.54 ± 0.04	7.2 ± 2.0		
	Zn-O	6	4.60 ± 0.04	3.0 ± 1.9		
Zn foil	Zn-Zn	6	2.65 ± 0.01	10.5 ± 3.8	0.8 ±0.4	0.80 ± 0.06
	Zn-Zn	6	2.78 ± 0.01	23.0 ± 2.0		
	Zn-Zn	6	3.92 ± 0.01	22.0 ± 1.6		
	Zn-Zn	6	4.61 ± 0.04	18.7 ± 6.0		
	Zn-Zn	12	4.77 ± 0.04	21 4 ± 3.7		
	Zn-Zn	6	5.15 ± 0.03	16.7 ± 3.7		
	Zn-Zn	12	5.52 ± 0.03	14 4 ± 1.7		

According to the fitting results listed in Table I, Zn does not form metallic clusters or ZnO precipitates. More specifically, both the coordination number and the nn distance, suggest that Zn is octahedrally coordinated forming oxo-complexes [26] which are sorbed predominately in the outer-sphere configuration. [33] The results are also supported by the direct comparison of the FT amplitudes in Figure 7b.

The X-ray Absorption Near Edge Structure (XANES) spectra of the Zn-HEU, the ZnO (Zn^{2+}) powder and metallic Zn are shown in Figure 7c. The position of the absorption edge in XANES spectra is affected by the oxidation state of the absorbing atom. As the oxidation state increases, the absorption edge usually shifts towards higher energies. [34] Furthermore, the spectrum of the Zn-HEU is significantly different from that of ZnO and Zn foil, while it exhibits strong similarities with the

spectra of octahedrally coordinated Zn. [35] Additionally, the position of the main peak above the absorption edge in the Zn-HEU sample is red-shifted by 1.0 eV relative to the corresponding peak of ZnO. This shift is consistent with an octahedral coordination of Zn^{2+} in the Zn-HEU sample verifying the results obtained from the extended part of the XAFS spectrum. [35]

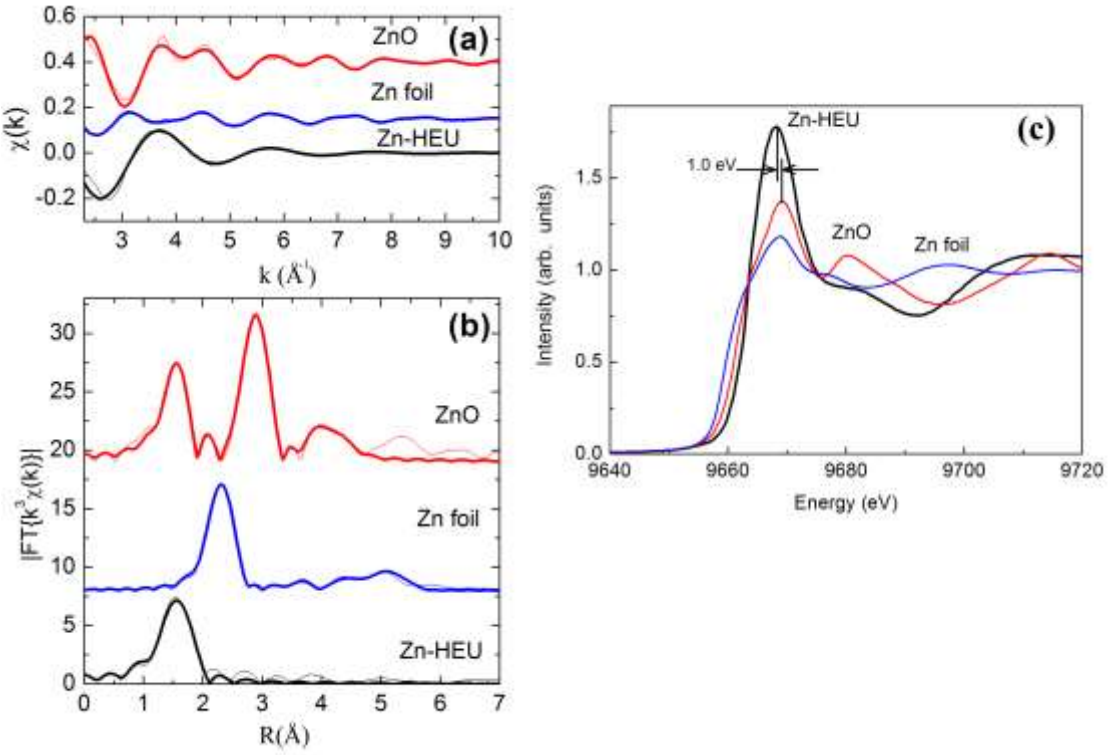

Figure 7: *(a) χ(k) and (b) corresponding Fourier Transform of the Zn-K-edge EXAFS spectra of Zn-HEU sample and a ZnO reference powder. The fitting and the experimental curves are shown in thick and thin solid lines, respectively. (c) Zn-K-edge XANES spectra of the Zn-HEU sample and a ZnO reference powder. The vertical lines indicate the shift between the most intense peaks in the spectra of the ZnO and Zn-HEU samples.*

To summarize, the EXAFS data in Table I evidences the absence of a Zn-Zn nearest neighbor distance, and the presence of a Zn-O nearest neighbor distance of 2.07 Å. This indicates that the *majority* of the Zn^{2+} ions is present as lone ions within the

HEU-type zeolite structure, and is octahedrally coordinated with oxygen. In Figure 5a, few small Zn clusters are imaged in the first TEM image. However, after just a short exposure to the electron beam, more clusters can be seen, and the clusters have started to grow. This demonstrates that the lone ions in the sample are highly mobile within the zeolite framework and can agglomerate extremely fast under electron beam irradiation. The speed at which the clusters form is similar, and possibly even faster than the damage mechanism of the electron beam to the zeolite framework (predominantly radiolysis).

4. Conclusions

The results presented above demonstrate the ability of aberration corrected transmission electron microscopy to characterize the framework structure of the natural HEU-type zeolite, as well as its interaction with guest metals. The HRTEM results for the Ag-HEU and Zn-HEU clearly indicate the presence of small Ag and Zn(O) clusters inside the zeolite structure. To further corroborate the TEM results, we performed electron tomography experiments which revealed the presence of Ag and Zn(O) material inside the zeolite structure and partially on the surface. Finally, in order to characterize the Zn^{2+} environment, we resorted to EXAFS measurements. The results demonstrate that the zinc cations in Zn-HEU arrange mainly in the form of small octahedral oxo-complexes.

Acknowledgements

GVT and MF acknowledge funding from the European Research Council under the 7th Framework Program (FP7), ERC grant N°246791 – COUNTATOMS. This work is also performed within the framework of the IAP-PAI.

The XAFS measurements at HZB were financially supported from the European Community's 7th Framework Program (FP7/2007-2013) under grant agreement No 226716. S.T. Gratefully acknowledges the Fund for Scientific Research Flanders (FWO). We would like to thank Prof. Nikolaos Kantiranis for performing the XRPD measurements and Dr. Maria Batuk for her assistance with the analysis of the XRPD measurements.

References

[1] A. Godelitsas, T. Armbruster, Microporous Mesoporous Mater. 61 (2003) 3.

[2] Ch. Baerlocher, L.B. McCusker, D.H. Olson, Atlas Zeolite Framework Types (2007) 156.

[3] N. Kantiranis, K. Sikalidis, A. Godelitsas, C. Squires, G. Papastergios, A. Filippidis, J. Environ. Manage. 92 (2011) 1569.

[4] A.S. Sheta, A.M. Falatah, M.S. Al-Sewailem, E.M. Khaled, A.S.H. Sallam, Microporous Mesoporous Mater. 61 (2003) 127.

[5] C.S. Lim, J.H. Ryu, J. Cryst. Growth 311 (2009) 486.

[6] B. Concepción-Rosabal, G. Rodríguez-Fuentes, N. Bogdanchikova, P. Bosch, M. Avalos, V.H. Lara, Microporous Mesoporous Mater. 86 (2005) 249.

[7] N. Fernández, S. Montalvo, R. Borja, L. Guerrero, E. Sánchez, I. Cortés, M.F. Colmenarejo, L. Travieso, F. Raposo, Renew. Energy 33 (2008) 2458.

[8] E. Alver, A.Ü. Metin, Chem. Eng. J. 200-202 (2012) 59.

[9] J. Hrenovic, J. Milenkovic, I. Goic-Barisic, N. Rajic, Microporous Mesoporous Mater. 169 (2013) 148.

[10] N. Döbelin, T. Armbruster, Am. Mineral. 88 (2003) 527.

[11] M. Ostroumov, P. Cappelletti, R. de'Gennaro, Appl. Clay Sci. 55 (2012) 27.

[12] O. Terasaki, T. Ohsuna, Topics in Catalysis, 24 (2003) 13.

[13] F. Gramm, C. Baerlocher, L.B. McCusker, S.J. Warrender, P.A. Wright, B. Han, S.B. Hong, Z. Liu, T. Ohsuna, O. Terasaki, Nature 444 (2006) 79.

[14] J. Sun, Z. He, S. Hovmöller, X. Zou, F. Gramm, C. Baerlocher, L.B. McCusker, Zeitschrift für Krist. 225 (2010) 77.

[15] H.W. Zandbergen, C.W.R. Engelen and J.H.C. van Hooff, Applied Catalysis, 25 (1986) 231.

[16] O. Terasaki, T. Ohsuna, V. Alfredsson, J.-O. Bovin, D. Watanabe and K. Tsuno, Ultramicroscopy 39 (1991) 238.

[17] J. C. Meyer, C. Kisielowski, R. Erni, M. D. Rossell, M. F. Crommie, Nanoletters 8 (2008) 3582.

[18] Z. Lee, J. C. Meyer, H. Rose, U. Kaiser, Ultramicroscopy 112 (2012) 39.

[19] S. Mintova, N. H. Olson, V. Valtchev and T. Bein, Science 283, 958 (1999)

[20] I. Diaz and A. Mayoral, Micron 42 (2011) 512.

[21] H. Förster, U. Hatje, Solid State Ionics 101-103 (1997) 425.

[22] L. Khouchaf, M.-H. Tuilier, M. Wark, M. Soulard, H. Kessler, Microporous Mesoporous Mater. 20 (1998) 27.

[23] Václav Petříček, Michal Dušek, Lukáš Palatinus, Zeitschrift für Kristallographie - Crystalline Materials 229 (1994) 345.

[24] J.M. Cowley, A.F. Moodie, Proc. Phys. Soc. 76 (1960) 378.

[25] S.P.B. Kremer, C.E.A. Kirschhock, A. Aerts, K. Villani, J.A. Martens, O.I. Lebedev, G. Van Tendeloo, Adv. Mater. 15 (2003) 1705.

[26] Š.C. Stefanović, N.Z. Logar, K. Margeta, N.N. Tušar, I. Arčon, K. Maver, J. Kovač, V. Kaučič, Microporous Mesoporous Mater. 105 (2007) 251.

[27] Z. Lee, K.-J. Jeon, A. Dato, R. Erni, T.J. Richardson, M. Frenklach, V. Radmilovic, Nano Lett. 9 (2009) 3365.

[28] C. Aydin, J. Lu, M. Shirai, N.D. Browning, B.C. Gates, ACS Catal. 1 (2011) 1613.

[29] P. A. Midgley, M. Weyland, Ultramicroscopy 96 (2003) 413.

[30] S. Bals, K. J. Batenburg, D. Liang, O. Lebedev, G. Van Tendeloo, A. Aerts, J. A. Martens, C. E. A. Kirschhock, J. Am. Chem. Soc. 131 (2009) 4769.

[31] M. Newville, B. Ravel, D. Haskel, J. J. Rehr, E. A. Stern, and Y. Yacoby, Physica B 208&209, (1995), 154

[32] J.J. Rehr, R.C. Albers, Rev. Mod. Phys. 72 (2000) 621.

[33] J. Ha, T.P. Trainor, F. Farges, G.E. Brown, Jr., Langmuir 25 (2009) 5574.

[34] J.-F. Wang, K.-X. Wang, J.-Q. Wang, L. Li, Y.-M. Jiang, X.-X. Guo, J.-S. Chen, J. Solid State Chem. 202 (2013) 111.

[35] C. Hennig, F. Thiel, K. Hallmeier, R. Szargan, A. Hagen, F. Roessner, Spectrochim. Acta A-Molecular and Biomolecular Spectroscopy 49A (1993) 1495.